Registration No.

26305

-Technical Report-

The Depth Limits of Eddy Current Testing for Defects: A Computational Investigation and Smooth-Shaped Defect Synthesis from Finite Element Optimization

Presented at 2015 SAE World Congress (Paper # 2015-01-0595), Detroit, MI, April 21-23, 2015

T Mathialakan[1], V U Karthik[1], S R H Hoole[1]
P Jayakumar[2], R Thyagarajan[2]

[1] *Michigan State University, Lansing, MI*
[2] *US Army TARDEC, Warren, MI*

Also published as a Journal paper:

CITATION: **Mathialakan, T., Karthik, V., Jayakumar, P., Thyagarajan, R. et al., "The Depth Limits of Eddy Current Testing for Defects: A Computational Investigation and Smooth-Shaped Defect Synthesis from Finite Element Optimization," SAE Int. J. Mater. Manf. 8(2):2015, doi:10.4271/2015-01-0595.**

[redacted]ment A
[redacted]305

22 April 2015

U.S. Army Tank Automotive Research, Development, and Engineering Center
Detroit Arsenal
Warren, Michigan 48397-5000

REPORT DOCUMENTATION PAGE

Form Approved
OMB No. 0704-0188

1. REPORT DATE *(DD-MM-YYYY)*	**2. REPORT TYPE**	**3. DATES COVERED** *(From - To)*
22 APRIL 2015	Conference and Journal Paper	10/01/2014 – 03/31/2015

4. TITLE AND SUBTITLE

The Depth Limits of Eddy Current Testing for Defects:
A Computational Investigation and Smooth-Shaped Defect Synthesis from Finite Element Optimization

5a. CONTRACT NUMBER
W56HZV-07-2-0001

5b. GRANT NUMBER
MOD P00009
W56HZV-08-C-0236

5c. PROGRAM ELEMENT NUMBER

6. AUTHOR(S)

T. Mathialakan, V. U. Karthik, S. Ratnajeevan H. Hoole

Paramsothy Jayakumar and Ravi Thyagarajan

5d. PROJECT NUMBER

5e. TASK NUMBER

5f. WORK UNIT NUMBER

7. PERFORMING ORGANIZATION NAME(S) AND ADDRESS(ES)

Michigan State University
E Lansing
MI 48224

TARDEC/Analytics
6501 E 11 Mile Road
Warren MI 48397

8. PERFORMING ORGANIZATION REPORT NUMBER

9. SPONSORING / MONITORING AGENCY NAME(S) AND ADDRESS(ES)

Sponsors:
TARDEC/Analytics
6501 E 11 Mile Road
Warren MI 48397

10. SPONSOR/MONITOR'S ACRONYM(S)
TARDEC

11. SPONSOR/MONITOR'S REPORT NUMBER(S)
#26305 (TARDEC)

12. DISTRIBUTION / AVAILABILITY STATEMENT
UNCLASSIFIED: Distribution Statement A. Approved for Public Release, Unlimited Distribution

13. SUPPLEMENTARY NOTES
Also published in the SAE Int. J. Mater. Manf. 8(2):2015, doi:10.4271/2015-01-0595.

14. ABSTRACT

This paper presents a computational investigation of the validity of eddy current testing (ECT) for defects embedded in steel using parametrically designed defects. Of particular focus is the depths at which defects can be detected through ECT. Building on this we characterize interior defects by parametrically describing them and then examining the response fields through measurement. Thereby we seek to establish the depth and direction of detectable cracks. As a second step, we match measurements from eddy current excitations to computed fields through finite element optimization. This develops further our previously presented methods of defect characterization. Here rough contours of synthesized shapes are avoided by a novel scheme of averaging neighbor heights rather than using complex Bézier curves, constraints and such like. This avoids the jagged shapes corresponding to mathematically correct but unrealistic synthesized shapes in design and nondestructive evaluation.

15. SUBJECT TERMS
Eddy Current testing, ECT, defect detection, NDE, defect characterization, parametrization, genetic algorithm, GPU, thread, magnetostatic

16. SECURITY CLASSIFICATION OF:			**17. LIMITATION OF ABSTRACT**	**18. NUMBER OF PAGES**	**19a. NAME OF RESPONSIBLE PERSON**
a. REPORT	**b. ABSTRACT**	**c. THIS PAGE**			Ravi Thyagarajan
Unlimited	Unlimited	Unlimited	Unlimited	12	**19b. TELEPHONE NUMBER** *(include area code)* 586-282-6471

Standard Form 298 (Rev. 8-98)
Prescribed by ANSI Std. Z39.18

TANK-AUTOMOTIVE RESEARCH
DEVELOPMENT ENGINEERING CENTER
Warren, MI 48397-5000

Ground Systems Engineering / Analytics
22 April 2015

The Depth Limits of Eddy Current Testing for Defects: A Computational Investigation and Smooth-Shaped Defect Synthesis from Finite Element Optimization

By

T Mathialakan[1], V U Karthik[1], S R H Hoole[1]
P Jayakumar[2], R Thyagarajan[2]

[1] *Michigan State University, E Lansing, MI*
[2] *US Army TARDEC, Warren, MI*

This is a reprint of a paper published in the SAE International Journal of Materials and Manufacturing (2015), and presented under the same title during the 2015 SAE World Congress, Apr 21-23, 2015 in Detroit, MI.

Distribution List

- Dr. Pat Baker, Director, ARL/SLAD, Aberdeen, MD
- Mr. Craig Barker, Program Manager, UBM/T&E, SLAD, US Army Research Lab
- Dr. Bruce Brendle, Deputy Executive Director, CSI, US Army TARDEC
- Mr. Robert Bowen, ARL/SLAD, Aberdeen, MD
- Mr. Ken Ciarelli, Deputy Executive Director, RTI, US Army TARDEC
- Dr. Kent Danielson, Engineer Research and Development Center (ERDC), Army Core of Engineers
- Mr. Paul Decker, Deputy Chief Scientist, US Army TARDEC
- Ms. Harsha Desai, Ground Systems Engineering Support, US Army TARDEC
- Mr. Matt Donohue, DASA/R&T, ASA-ALT
- Dr. Jay Ehrgott, Engineer Research and Development Center (ERDC), Army Core of Engineers
- Ms. Nora Eldredge, WMRD, US Army Research Lab
- Mr. Ed Fioravante, WMRD, US Army Research Lab
- Mr. Mark Germundson, Deputy Associate Director, TARDEC/GSS
- Mr. Neil Gniazdowski, WMRD, US Army Research Lab
- Dr. David Gorsich, Chief Scientist, US Army TARDEC
- Mr. Dave Gunter, Acting Associate Director, Analytics, US Army TARDEC
- Dr. Dave Horner, Director, DoD HPC Mod Program
- Mr. Steve Knott, Deputy Executive Director, Systems Engineering, US Army TARDEC
- Mr. Jeff Koshko, Associate Director, TARDEC/GSS, US Army TARDEC
- Dr. Scott Kukuck, PM/Blast Institute, WMRD, US Army Research Lab
- Dr. Paramsothy Jayakumar, STE/Analytics, US Army TARDEC
- Mr. Mark Mahaffey, ARL/SLAD, Aberdeen, MD
- Dr. Tom McGrath, US Navy NSWC-IHD
- Dr. Thomas Meitzler, STE, TARDEC/GSS
- Mr. Micheal O'Neil, MARCOR SYSCOM, USMC
- Mr. Mark Simon, Survivability Directorate, US Army Evaluation Center
- Mr. Pat Thompson, US Army Testing and Evaluation Command (ATEC)
- Mr. Madan Vunnam, Team Leader, Analytics/EECS, US Army TARDEC
- Dr. Jeff Zabinski, Acting Director, WMRD, US Army Research Lab
- TARDEC TIC (Technical Information Center) archives, US Army TARDEC
- Defense Technical Information Center (DTIC) Online, http://dtic.mil/dtic/

2015-01-0595
Published 04/14/2015

doi:10.4271/2015-01-0595
saematman.saejournals.org

The Depth Limits of Eddy Current Testing for Defects: A Computational Investigation and Smooth-Shaped Defect Synthesis from Finite Element Optimization

T. Mathialakan and V. U. Karthik
Michigan State University

Paramsothy Jayakumar and Ravi Thyagarajan
US Army Tank Automotive

S. Ratnajeevan H. Hoole
Michigan State University

ABSTRACT

This paper presents a computational investigation of the validity of eddy current testing (ECT) for defects embedded in steel using parametrically designed defects. Of particular focus is the depths at which defects can be detected through ECT. Building on this we characterize interior defects by parametrically describing them and then examining the response fields through measurement. Thereby we seek to establish the depth and direction of detectable cracks. As a second step, we match measurements from eddy current excitations to computed fields through finite element optimization. This develops further our previously presented methods of defect characterization. Here rough contours of synthesized shapes are avoided by a novel scheme of averaging neighbor heights rather than using complex Bézier curves, constraints and such like. This avoids the jagged shapes corresponding to mathematically correct but unrealistic synthesized shapes in design and nondestructive evaluation.

CITATION: Mathialakan, T., Karthik, V., Jayakumar, P., Thyagarajan, R. et al., "The Depth Limits of Eddy Current Testing for Defects: A Computational Investigation and Smooth-Shaped Defect Synthesis from Finite Element Optimization," *SAE Int. J. Mater. Manf.* 8(2):2015, doi:10.4271/2015-01-0595.

INTRODUCTION

Eddy current testing (ECT) is a widely accepted, cheap and portable method for the detection of cracks and other defects in conductive materials. While ECT is a favorite with engineers for surface defect identification through nondestructive evaluation (NDE), for more deeply embedded defects the literature is not clear. It has been established that low frequency testing can distinguish "all the different levels" of corrosion when a sample is exposed to a very corrosive environment for 3 months [1] while other researchers have established that eddy current testing can identify corrosion to depths down to 15 mm [2, 3]. Submarines and aircraft employ eddy current probes for testing thin (up to 1 inch) conducting systems [4], and ultrasound [5] for thicker submarine hulls [6]. For deeper penetration, pulsed eddy currents [7] or remote field eddy currents are used [8, 9]. ECT Technology is therefore perfect for the purpose at hand.

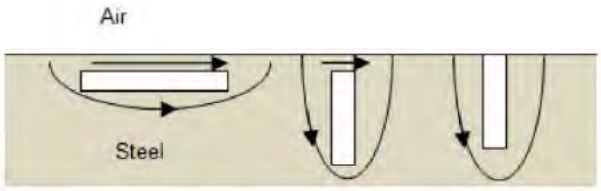

Fig.1. Penetration of Eddy Currents in the Presence of Defects

However, the reality is that, thinking qualitatively about the three situations in Fig.1, the depth for detection depends on defect orientation. In the first, when a defect is parallel to the surface, the defect will be detectable through the interruption of the eddies. In the second situation, it is perpendicular to the surface but not reaching the surface; we would expect the skin-effect to allow the currents to flow along the surface. So it will be hard to detect the defect in the second case. Whereas in the third situation if the defect is perpendicular to the surface without a gap for the eddy current to flow along the surface, the defect would interrupt the flow of eddy currents which would find it difficult to go deep

because of the skin effect. Therefore this will be easily detectable. On the other hand if the defect is thin and long, a 3D model will show no current interruption.

This interruption would make the presence of defects easily detectable. Different types of defect models with the ECT coil are shown in Fig.2. Defects a, b, c, d & e in Fig.2 show the difference in angle, depth and length. Moreover, if the axis of the external exciting ECT coil is parallel to the surface, our considerations need to be entirely different. This study therefore through a series of finite element analyses of parameterized geometries of a single defect, seeks to identify the limits of eddy current testing in NDE. This study is confined to steel plates for army ground vehicle armor. A qualitative relationship between the depth of a detectable defect, the frequency of excitation and the geometric parameters is sought to help engineers choose whether or not to use ECT.

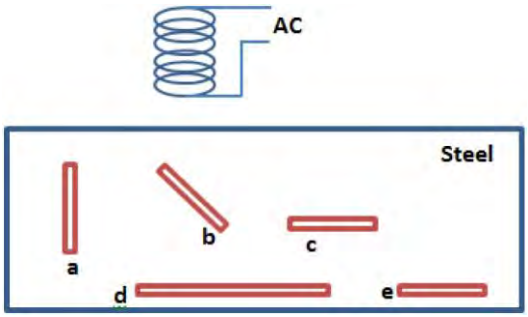

Fig.2. Defect Model: The model has defects in different angle (a, b, c), depth (c, e), and length (d, e).

DETECTION OF DEFECT: FIELD CHANGES

A defect in a material can be varied in shape and location. The defect detection method should concentrate on the characteristics of the defect. These effects are analyzed in this paper for varying size, shape and location of defect in materials. An iterative approach is presented that repeatedly employs the finite element technique for modeling the forward problem to calculate the effect caused by the defects in a steel plate.

We calculate the magnetic field density for the known defects from the forward problem using the finite element method [2] and examine the extent to which the exterior field is altered by the defect to see if the presence of the defect can be discerned through the changes in the measurable external field.

PROBLEM STATEMENT

Magnetic fields in a ferromagnetic material can be generated by placing an AC (Alternative Current) coil on top of the material. For AC magnetization, the vector magnetic potential **A**, and the exciting current density **J** at angular frequency ω, are related by

$$-\nabla \times \frac{1}{\mu} \nabla \times \boldsymbol{A} = \boldsymbol{J} - j\omega\sigma\boldsymbol{A} \quad (1)$$

where μ is the spatial permeability distribution and σ is the conductivity. The magnetic flux density **B** is related to the magnetic vector potential as,

$$\nabla \times \boldsymbol{A} = \boldsymbol{B} \quad (2)$$

In two dimensional problems, the current density **J** and the magnetic vector potential **A** will be in the $\hat{z}$ direction (i.e. the transverse direction in which no changes occur). Therefore the magnetic field density **B** will be in the $\hat{x}$ and $\hat{y}$ directions. From (1) and (2) we can write,

$$\frac{\partial}{\partial x}\left(\frac{\partial A}{\mu \partial x}\right) + \frac{\partial}{\partial y}\left(\frac{\partial A}{\mu \partial y}\right) + \boldsymbol{J} = 0 \quad (3)$$

Finite element analysis [10] provides the solution to (1) by applying certain boundary conditions. This leads to the finite element matrix equation

$$[\mathrm{P}]\{A\} = \{\mathrm{R}\} \quad (4)$$

where [P] is the finite element stiffness matrix and {R} is a column vector.

Any defect in the material should affect the magnetic field density **B** between the AC coil and the material. The magnetic field **B** is calculated at a line called the measuring line which is divided into m points. The effect in **B** caused by the defect for the *m* measuring points can be calculated using the expression

$$R^{B}_{(\theta,d,l)} = max_{i=0..m}\left(\left|\frac{B^{i}_{nodefect} - B^{i}_{defect}}{B^{i}_{nodefect}}\right|\right) \quad (5)$$

$R^{B}_{(\theta,d,l)}$ is the maximum value of flux ratio between flux changes and flux without the defect, where a defect with length *l* is at depth *d* from the material surface and rotated by angle θ clock-wise from the "horizontal" line parallel to the steel surface.

METHODOLOGY

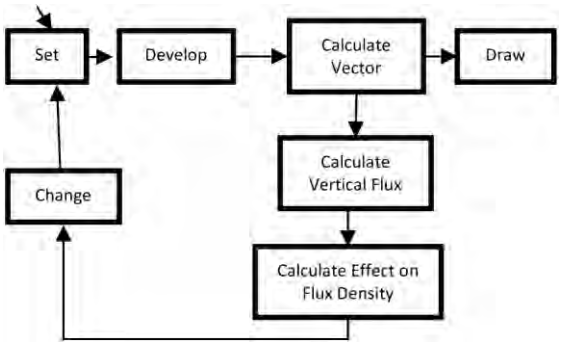

Fig.3. Design Cycle for the computation process

The computational process in the defect identification system is shown in Fig.3. It calculates the effect on the flux density for different kinds of defect that vary in their characteristics: depth (d), angle (θ) and length (l). The characteristics of a defect are the changing parameters in each calculation of the above computational process. In the latter part of our work, we extend this model for design optimization. Mesh generation is a very important part of finite element analysis based design optimization. We need to use a parameter based mesh generator, because in each iteration the mesh has to be generated automatically when design parameters change. Therefore we use a special script-based parametric mesh generator [11] using as backend the single problem mesh generator Triangle [12] to get the corresponding finite element solution for the magnetic vector potential **A**. Then from **A**, we compute the magnetic field density **B**. From **B** we calculate the effect on the flux density $R^{B}_{(\theta,d,l)}$. In each iteration, the electric field map is also generated and analyzed visually.

APPLICATION

The numerical example in Fig.4 is used to validate the proposed algorithm. The coil (with $\mu_r = 1.0$, current density $J = \pm 1\ A/m^2$, and $\omega = 10\ rad/s$) excites the magnetic field in the steel plate (with $\mu_r = 100.0$ and current density $J = 0.0$). The conductor is surrounded by air (with $\mu_r = 1.0$ and current density $J = 0.0$). The magnetic field density in the $\hat{y}$ direction B_y is calculated at 10 points as shown in Fig.4. labeled as the measuring line.

First, B_y for the steel plate with no defect is calculated at the measuring line and named $B_{nodefect}$. Since our study is about whether the defect is detectable or not, we defined a single defect with parameterized geometries {x, d, l, w, θ} (Fig.4.).

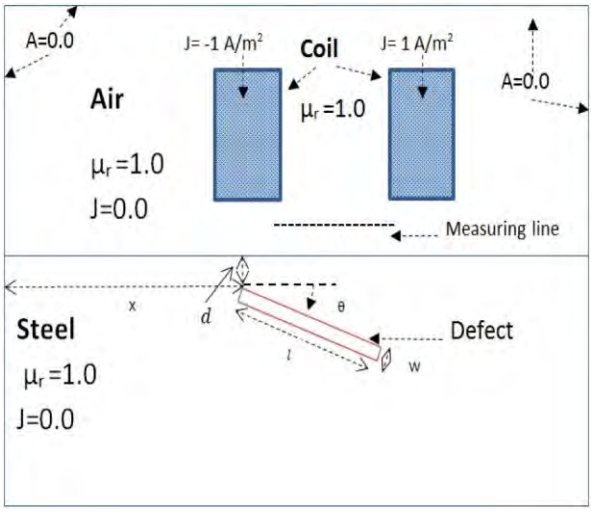

Fig.4. Numerical Model

By changing the parameters of the defect, we change the position of the defect as shown in Fig.5. and calculate By at the measuring points, which we name B_{defect}. Then the effect on flux density $R^{B}_{(\theta,d,l)}$ was calculated for each defect and tabulated. By considering the maximum of R, we establish the defect detecting quantity which is measured.

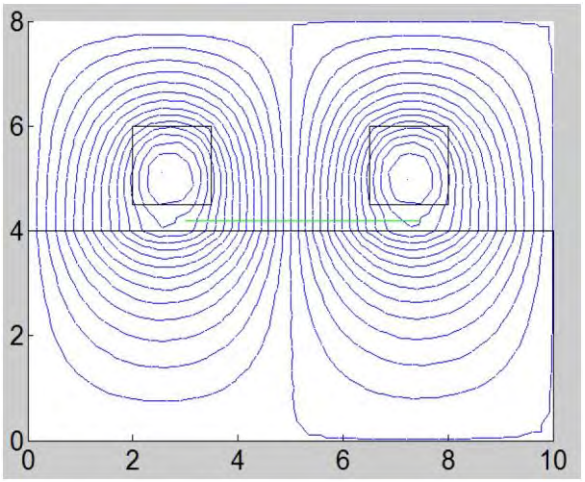

a. No defect

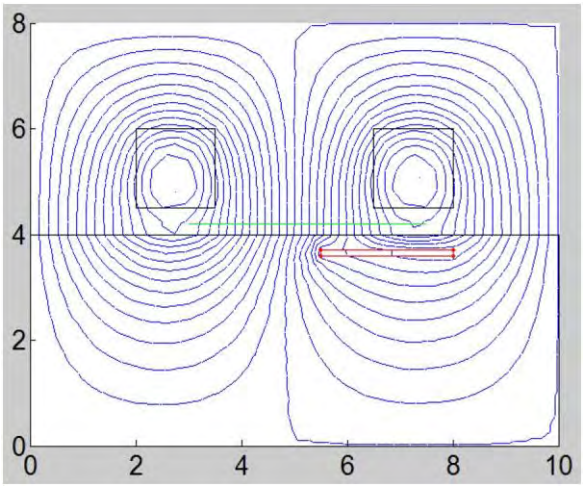

b. $d = 0.3$ and $\theta = 0$

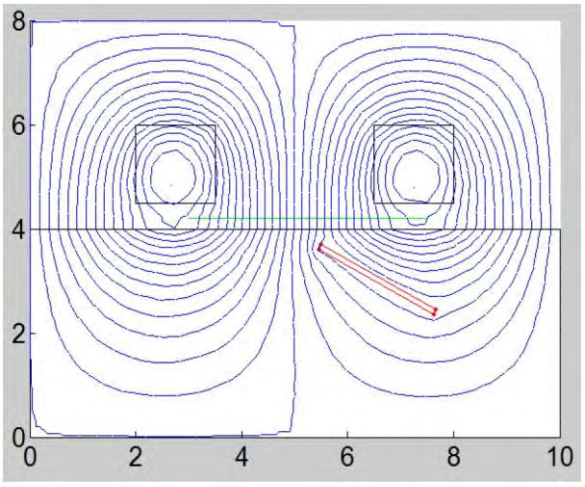

c. $d = 0.3$ and $\theta = 30$

Fig.5. Equipotential lines for the defects at various positions

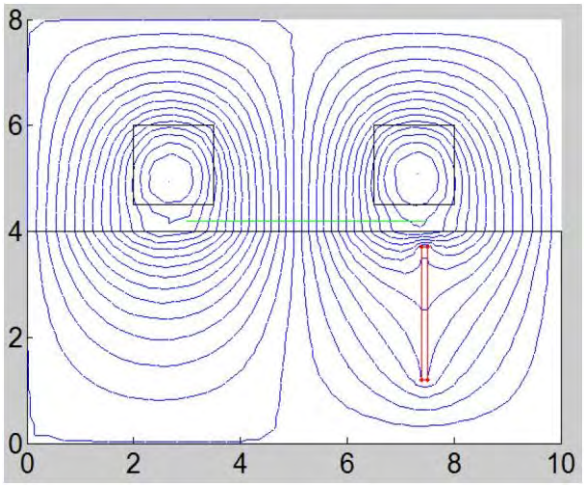

d. $d = 0.3$ and $\theta = 90$

Fig.5. (cont.) Equipotential lines for the defects at various positions

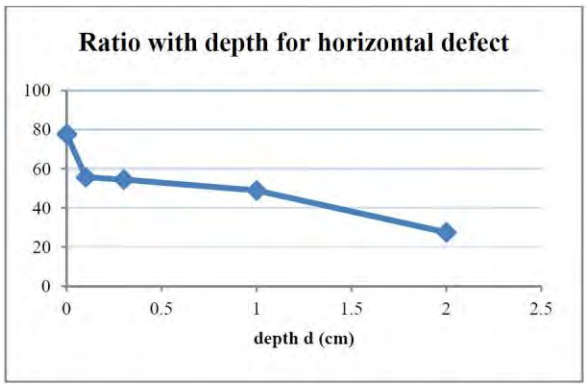

a. $R^B_{(\theta,d,l)}$ varies with d for horizontal defect

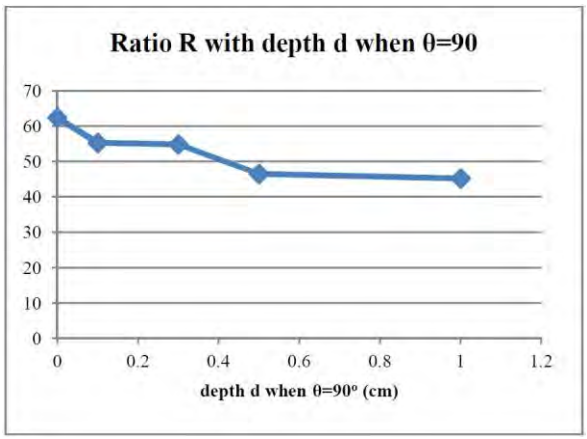

b. $R^B_{(\theta,d,l)}$ varies with d for vertical defect

Fig.6.

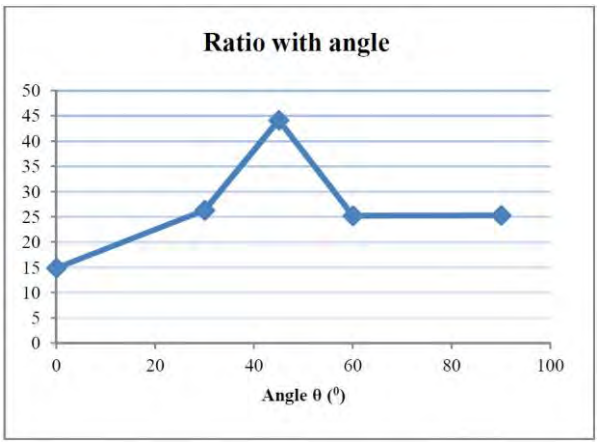

c. $R^B_{(\theta,d,l)}$ varies with θ

Fig.6. (cont.) $R^B_{(\theta,d,l)}$ with defect location

Fig.6. shows how the ratio $R^B_{(\theta,d,l)}$ varies with defect locations. When $R^B_{(\theta,d,l)}$ is high, there is a higher chance that the defect will be detected. Fig 6.a shows the results for a horizontal defect ($\theta = 0°$.) when the depth d increases: $R^B_{(\theta,d,l)}$ decreases. So that means when the depth of the defect is higher, it would be harder to detect as to be expected. Fig 6.b shows when the defect is vertical ($\theta = 90°$) how $R^B_{(\theta,d,l)}$ varies with depth. Here also when d increases $R^B_{(\theta,d,l)}$ decreases. Here $d = 0$ corresponds to the right-most part of Fig.1. Anyway when we compare a horizontal defect and vertical defect, the horizontall defect has a higher chance to be detected. This is to be expected because a horizontal defect will interrupt flux more since the flux flow is along the surface. Fig.6.c shows how $R^B_{(\theta,d,l)}$ varies with angle θ: $R^B_{(\theta,d,l)}$ goes to a maximum when $\theta = 45°$. So we could say that when the angle of the defect is 45°, there is higher chance to be detected.

Experimental work was done to verify the computational work of defect detection. The coil was moved along the x axis of the steel plate (Fig.7.b.) and the voltage induced was measured as shown in Fig.7. We created a rectangular defect on a steel plate. As shown in Fig.7.a. A close-up look of the defect is shown in Fig.7.b. Alternative sinusoidal current was excited in the coil with 300 mV at 20 kHz using the waveform generator. A pick up coil was wound on top of the AC coil to measure the voltage induced. Since the voltage induced is very small, we used the lock-in amplifier to measure voltage. We moved the coil along the surface of the steel and measured the induced voltage at the measuring points indicated on Fig.7. According to Faraday's equation, the voltage induced V_{ind} is proportional to the change in flux φ (6).

The results were tabulated and plotted in Fig. 8. From the plot, when the coil is just above the defect, the voltage induced is at its maximum. The test was repeated with different input voltages and different frequency and we obtainedt the same behavior as Fig.8. In this way we could detect the defects and moved to the defect characterization part of this study. The frequency of excitation also plays an important role in detecting the defect. As in equation (6), when frequency ω goes high, V_{ind} will be high and can be measured easily. But the eddy current will flow close to the surface due to the skin effect. Therefore we cannot detect defects which are deeply inside the plate. Our lock-in amplifier (Model SR844) has a bandwidth of 20 kHz to 200 MHz. Due to the limitation of

resources; we could not experiment with low frequencies. We did our work using 20 kHz, the lowest frequency that we can use to measure the readings.

EXPERIMENTAL WORK

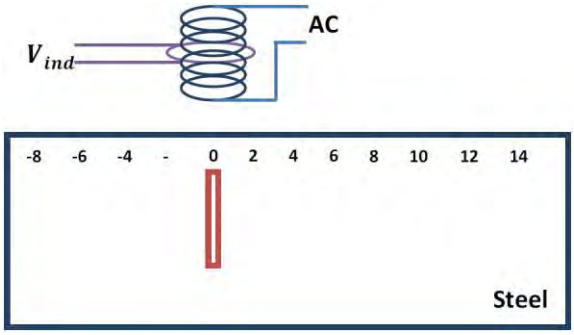

Fig.7. Experimental setup

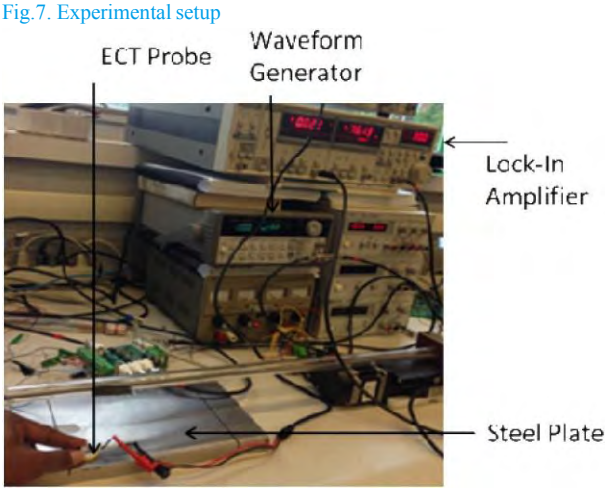

Fig.7.a. Lab setup

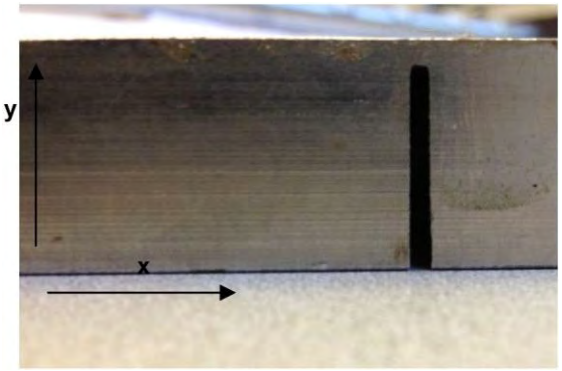

Fig.7.b. Close-up-look of the defect

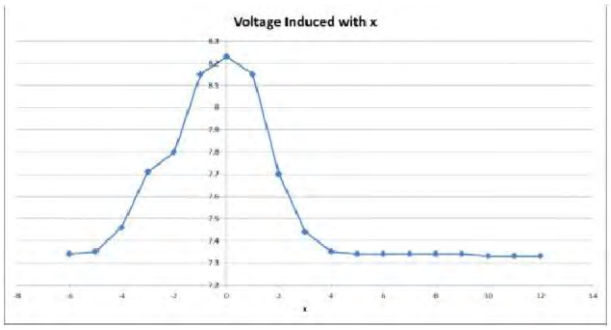

Fig.8. Voltage induced on pickup coil

$$V_{ind} \propto j\omega\varphi \tag{6}$$

DEFECT CHARACTERIZATION

After detecting the defect, we investigated more on defect characterization. It is important to know the size or character of the defect after establishing that there is defect inside. So in our work we investigate and establish a procedure for defect characterization so that a decision to withdraw a defective part may be thought-out, justifiable.

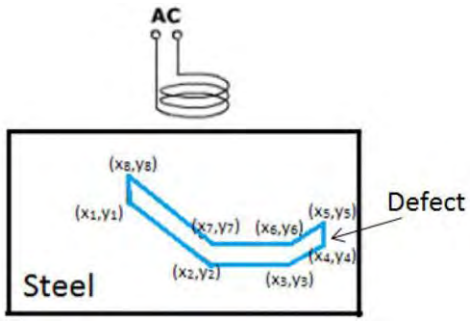

Fig.9. Defect Model

The methodology at present [13] examines the response of the hull under test to an excitatory signal from an eddy current probe. By knowing the response when there is no defect, if the response is different because of the defect, the test object is presently flagged as defective and the plate is sent for repairs without assessing if the defect is serious enough for removal from service. In our work, we extend that methodology to defect characterization. An iterative approach is presented that repeatedly employs the finite element technique for modeling the forward problem to characterize the shape of defects in a steel plate.

We can calculate the magnetic field density for the known defects from the forward problem. But in our inverse problem we need to know the characteristics of the defect for that field configuration. In design optimization, the problem geometry is defined in terms of design parameters contained in a vector $\bar{h} = \{x_1, y_1, \ldots, x_n, y_n\}$ (Fig.9.). An objective function F is defined as the sum of the squares of the difference between computed and measured (defect) performance values: at measurement points i,

$$F(x_1, y_1, .., y_n) = \sum_i \left(\mathbf{B}^i_{\text{Calculated}} - \mathbf{B}^i_{\text{Measured}}\right)^2 \tag{5}$$

F is a function of defect shape. By minimizing the objective function F with respective to the parameters by any of the optimization methods, the characteristics of the defect can be estimated.

The computational process in inverse problem solution is shown in Fig.10. It requires solving for the vector of design parameters $\bar{h}$. We first generate the mesh from the latest parameter set $\bar{h}$ to get the corresponding finite element solution for **A** and then compute **B**.

From **B** we evaluate the objective function F. The method of optimization used will dictate how the parameter set of device description $\bar{h}$ is to be changed depending on the computed F.

Zeroth order optimization is practicable in terms of avoiding the horrendous programming complexity of first order optimization although computations are extensive [14]. The Genetic Algorithm (GA) which is a zeroth order optimization method is good at handling potentially huge search spaces.

Its fitness score f is defined in terms of the object function F. Although our object function F as defined in (5) is to be minimized, the fitness score f has to be maximized for the genetic algorithm. We therefore define the fitness score

$$f = \frac{1}{1+F} \tag{6}$$

According to the methodology of optimization using GA as shown in Fig.11. first we randomly generate hundreds of vectors $\bar{h}$ (each called a chromosome) and this set is termed the initial population. With parallels to evolution, a new generation is to be created based on the best of this population.

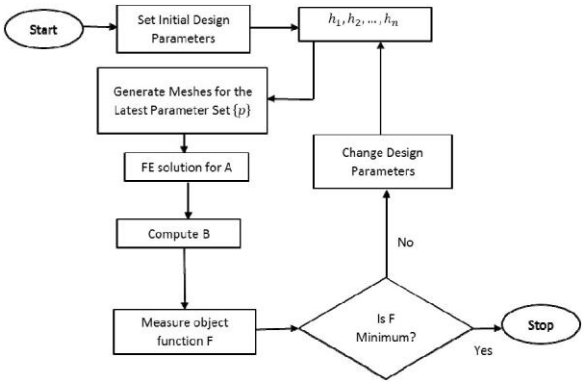

Fig.10. Design Cycle for the computation process

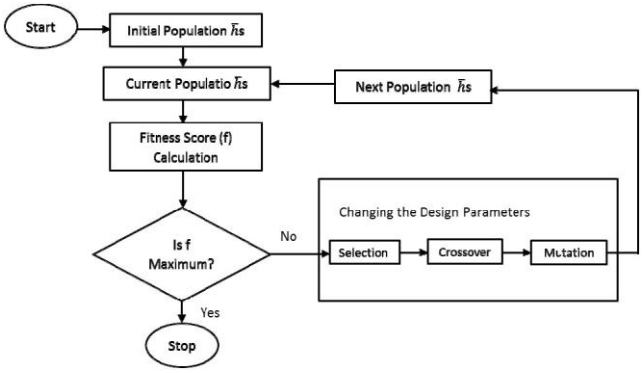

Fig.11. Optimization Using the Genetic Algorithm

Then the fitness score for each $\bar{h}$ is calculated and checked as to whether there is a score at 1 or close enough for our purposes. This computation involves computing F according to (5) and therefore a finite element solution for that $\bar{h}$. If there is no f satisfactorily close to 1, then the design parameters are changed according to the GA's classical way of selection, namely selection, crossover, and mutation Another reason for using GA is that it is also inherently parallel so that it may be easily adapted to computations on the graphics processing unit [15] Though GA is practicable and gives a better solution, it is slow when compared with the gradient optimization methods. Therefore NVidia GPU parallel computing architecture can be used to solve our problem. In our normal programming (single CPU), the fitness value is calculated for each chromosome $\bar{h}$ one by one. When the population is high it takes a very long time to converge. Therefore we launched kernels on fitness value calculation. For that we launched GPU threads and blocks of the same number as the population size (N) so that the fitness value will be calculated simultaneously for each chromosome in the population as shown in Fig.12. Therefore in this paper, we evaluate the proposed algorithm by applying the GA to a numerical NDE problem.

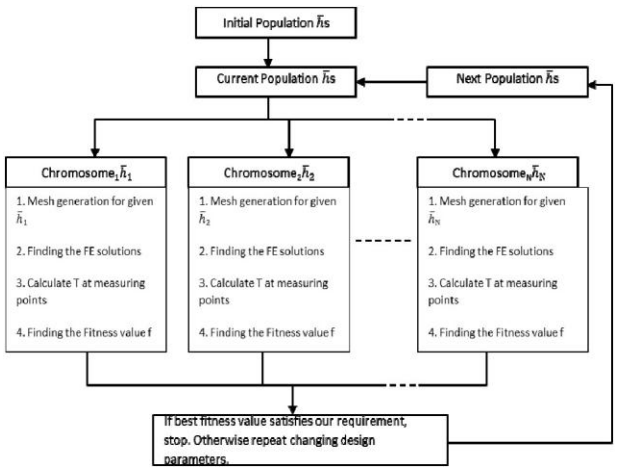

Fig.12. The Parallelized Process of the GPU [15]

NUMERICAL MODEL

The numerical example in Fig.13. is used to validate the proposed algorithm. The coil (with μ_r = 1.0, and current density J = ± 5 × 10^4 A/m^2) excites the magnetic field in the steel plate (with μ_r = 100.0 and current density J = 0.0). The conductor is surrounded by air (with μ_r = 1.0 and current density J = 0.0). The magnetic field density in the $\hat{y}$ direction B_y is measured at y = 4.5 cm, 8 cm ≤ × ≤ 12 cm using 10 points in the interval as shown in Fig.13. labeled as the measuring line.

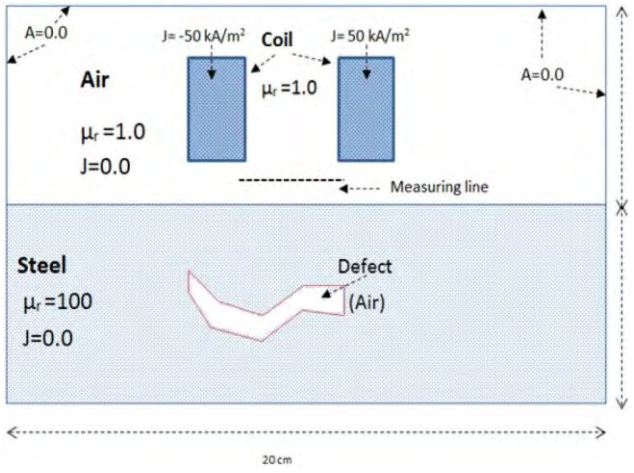

Fig.13. Numerical Model for defect characterization

On each node on the defect, the vertical displacements are selected as design parameters. In our numerical model we have 8 geometric parameters contained in the vector $\bar{h}$ $(y_1, y_2, y_3, y_4, y_5, y_6, y_7, y_8)$. The measuring line located at y = 4.5 cm, is sampled into 10 equally spaced points and tolerance boundaries are set to 0.5 cm ≤ h ≤ 3.5 cm. Each design variable is represented by 10 bits. For testing we took a particular defect $\bar{h}$ as $\bar{h}$ = {2.0, 1.2, 2.4, 2.2, 2.7, 3.0, 3.2, 3.5} cm and computed the field ($B_{Measured}$).

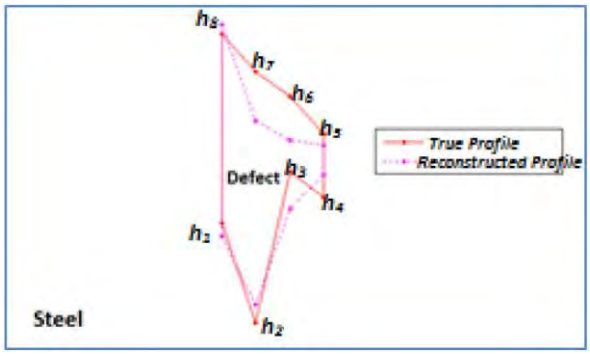

Fig.14. Optimum shape of the Reconstructed Defect

Now our algorithm has to reconstruct $\bar{h}$ to match the "measurements" ($B_{Measured}$). Design parameters are changed in every iteration and the infinite element mesh newly generated. After computing A by finite elements the magnetic field ($B_{Calculated}$) is computed and the objective function F is evaluated. When the object function F is minimum the iterations are stopped and $\bar{h}$ is found. Fig.14. shows the optimum shape of the defect after 200 iterations for a population size of 200. This shows a 70% accurate reconstruction of the defect. This error is computed from the equipotential lines for the finite element solution of the magnetic vector potential Fig.15.

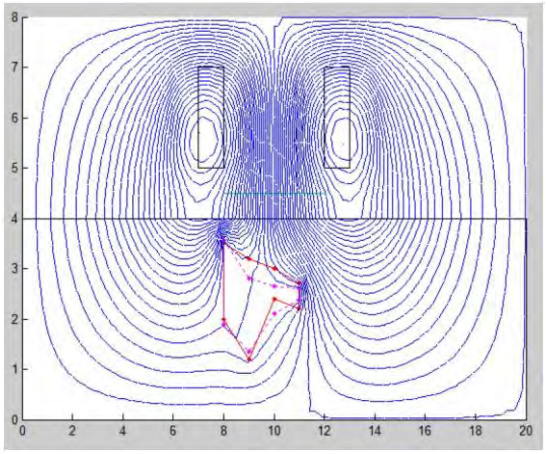

Fig.15. Solutions in Equipotential lines for the Numerical Model

SMOOTH-SHAPED DEFECT

In inverse problem design optimization, getting a practically manufacturable shape is important. An erratic undulating shape with sharp edges arose when Pironneau optimized a pole face to achieve a constant magnetic flux density [16]. Their results are shown in Fig.16. The nonsmooth jagged contour in Fig.16b. that they realized is practically not a manufacturable shape. This they addressed by smoothening the pole face as in Fig.16c manually.

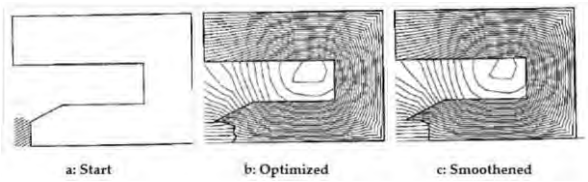

Fig.16. Jagged Pole Face of Right Half of Recording Head [17].

In our more generalized numerical shape synthesis, the problem of jagged shapes was overcome by imposing constraints [18]. In a subsequent paper to smoothen a surface we took the final result and set the coordinates of each point on a surface being shaped to the average of that node's coordinates and those to its left and right [19]. We also used element by element matrix solution to speed up the solution process [20].

Since our design optimization is for defect characterization, there is no need to impose constraints to get a smooth manufacturable shape. But we have to get a single defect with a realistic shape to estimate whether or not to pull the vehicle bearing that defective hull out of service. In this instance however, so as to maintain a realistic shape with a single defect we imposed the constraints as $h_8 > h_1$; $h_7 > h_2$; $h_6 > h_3$; and $h_5 > h_4$; Here in the inequality the left term represents the upper surface of the postulated defect and the right term the lower surface. In effect these inequalities ensure that the surfaces do not cross each other. Therefore we could get single and realistic defect as shown in Fig.15.

CONCLUSION

According to our investigation when the depth of the defect increases, it is hard to detect. We also found that when we compare horizontal and vertical defects, that a horizontal defect has a higher chance of being detected. While these results might be intuitive, a surprising finding is that our results showed that when a defect is at an angle of 45° from the surface, it has a higher chance of being detected.

This paper also presents a finite element technique for solving inverse problems in magnetostatic NDE. Defect shape reconstructing using the genetic algorithm optimization method is presented and validated using a numerical model. We also imposed constraints in the system to get a realistic single defect reconstruction that is smooth.

REFERENCES

1. Alamin M., Tian G.Y., Andrews A., and Jackson P., "Corrosion Detection using Low-Frequency RFID Technology," *INSIGHT*, Vol. 54, No. 2, pp. 72-75, Feb. 2012.
2. Yamada Hironobu, Hasegawa Teruki, Ishihara Yudai, Kiwa Toshihiko, and Tsukada Keiji, "Difference in the detection limits of flaws in the depths of multi-layered and continuous aluminum plates using low-frequency eddy current testing," *NDT&E International*, Vol. 41, pp. 108-111, 2008.
3. Skramstad J., Smith R.A., and Edgar D., "Enhanced Detection of Deep Corrosion using Transient Eddy Currents," Proc. Seventh Joint DoD/ FAA/NASA Conference on Aging Aircraft, New Orleans, Sept. 2003.

4. Joshi A.V., Udpa L., and Udpa S.S., "Use of higher order statistics for enhancing magnetic flux leakage pipeline inspection data," *Int. J. App. Electromag. & Mechanics*, Vol. 25, No. 1-4, pp. 357-362, 2007.
5. Kubinyi, A. Docekal, Ramos H.G., and Ribeiro A.L., "Signal Processing for Non-contact NDE," *PRZEGLĄD ELEKTROTECHNICZNY*, Vol. 86, No. 1, 2010.
6. Guang, Tamburrino A., Udpa L., Udpa S.S., Zeng Z., and Deng Y , "Pulsed eddy current based GMR system for the inspection of aircraft structures," *IEEE Trans. Magn*., Vol. 46, pp. 910-917, 2010.
7. Liu Zheng, Ramuhalli Pradeep, Safizadeh Saeed and Forsyth David S, "Combining multiple nondestructive inspection images with a generalized additive model," *Meas. Sci. Technol*. 19 (2008) 085701 (8pp)
8. Lord W , Sun Y. S., Udpa S. S. and Nath S., "Finite element study of the remote field eddy current phenomenon," IEEE Trans. Magn., Vol. 24, No. I, pp. 435-438, Jan. 1988.
9. Schmidt T. R., "The remote field eddy current inspection techniques," Materials Evaluation, Vol. 42, pp. 225-230, Feb. 1984.
10. Hoole S. R. H., *Computer-Aided Analysis and Design of Electromagnetic Devices*, Elsevier, New York, 1989.
11. Sivasuthan S., Karthik V. U., Rahunanthan A., Jayakumar P., Thyagarajan Ravi, Udpa Lalita and Hoole S.R.H., "GPU Computation: Why Element by Element Conjugate Gradients?," The Sixteenth Biennial IEEE Conference on Electromagnetic Field Computation, Annecy, 2014.
12. Shewchuk Jonathan Richard, Triangle: Engineering a 2D Quality Mesh Generator and Delaunay Triangulator, in *Applied Computational Geometry Towards Geometric Engineering* Lin (Ming C. and Manocha Dinesh, editors), volume 1148 of Lecture Notes in Computer Science, pages 203-222, Springer-Verlag, Berlin, May 1996.
13. Yan, M.; Udpa, S.; Mandayam, S.; Sun, Y.; Sacks, P.; Lord, W., "Solution of inverse problems in electromagnetic NDE using finite element methods," Magnetics, IEEE Transactions on, vol.34, no.5, pp.2924,2927, Sep 1998
14. Preis K., Magele C. and Biro O., "FEM and Evolution Strategies in the Optimal Design of Electromagnetic Devices," IEEE Trans. Magnetics, Vol. 26(5), pp. 2181-2183, Sept. 1990.
15. Karthik Victor U., Sivasuthan Sivamayam, Rahunanthan Arunasalam, Thyagarajan Ravi S., Jayakumar Paramsothy, Udpa Lalita, and Hoole S. Ratnajeevan H., "Faster, more accurate, parallelized inversion for shape optimization in electroheat problems on a graphics processing unit (GPU) with the real-coded genetic algorithm," COMPEL - Int. J. Comput. Math. Electr. Electron. Eng., vol. 34, no. 1, pp. 344-356, Jan. 2015.
16. Pironneau, O. (1984), Optimal Shape Design for Elliptic Systems, Springer-Verlag, New York, 1984.
17. Marrocco A. and Pironneau O., "Optimum Design with Lagrangian Finite Elements: Design of an Electromagnet," *Computer Methods in Applied Mechanics and Engineering*, Vol. 15, pp. 277-308, 1978.
18. Subramaniam, S., Arkadan, A.A. and Hoole, S.R.H. (1994), "Optimization of a magnetic pole face using linear constraints to avoid jagged contours "Constraints for Smooth Geometric Contours from Optimization," IEEE Trans. Magn., Vol. 30 (5), pp. 3455-3458.
19. Sivasuthan, S., Karthik, V.U., Rahunanthan, A., Jayakumar, P., Thyagarajan Ravi S., Ravi S., Udpa, Lalita and Hoole, S.R.H., "A Script-based Parameterized Finite Element Mesh for Design and NDE on a GPU," *IETE Technical Review*, DOI: 10.1080/02564602.2014.983192, Prepress published on line 23 Dec. 2014.
20. Sivasuthan, S., Karthik, V.U., Rahunanthan, A., Jayakumar, P., Thyagarajan Ravi S., Ravi S., Udpa, Lalita and Hoole, S.R.H., "Addressing Memory and Speed Problems in Nondestructive Defect Characterization: Element-by-Element Processing on a GPU," *Int. Journ. Nondestructive Evaluation*. Accepted subject to revision.

DISCLAIMER

UNCLASSIFIED: Distribution Statement A. Approved for public release. #26305